Supplementary Material

On the origin of metallicity and stability of the metastable phase in chemically exfoliated MoS_2

Debasmita Pariari [a], Rahul Mahavir Varma [a], Maya N. Nair [a,+], Patrick Zeller [b], Matteo Amati [b], Luca Gregoratti [b], Karuna Kar Nanda [c], D. D. Sarma [a,*]

[a]*Solid State and Structural Chemistry Unit, Indian Institute of Science, Bengaluru 560012, India*

[b]*Elettra-Sincrotrone Trieste S.C.p.A., SS14, km 163.5 in AREA Science Park, 34149 Basovizza, Trieste, Italy*

[c]*Materials Research Centre, Indian Institute of Science, Bengaluru 560012, India*

[*]Corresponding author: sarma@iisc.ac.in

[+]Present address: CUNY Advanced Science Research Center, 85 St. Nicholas Terrace, New York, NY 10031, USA

1. Structure of undistorted (T) and distorted (T′) octahedral phase:

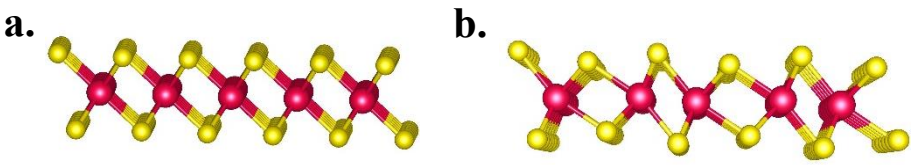

Fig. S1. Side views of (a) T and (b) T′ phase of MoS_2 where red and yellow balls indicate Mo and S atoms, respectively.

Six S atoms are arranged around a Mo atom in a pure and distorted octahedral fashion in T and T′ phases, respectively. For the T phase, Mo-Mo distance is same throughout the chain in contrast to the T′ phase, where dimerization of consecutive Mo atoms lead to the formation of zigzag arrangements of the Mo ions. The side views for both T and T′ phases are shown in Fig. S1a and b. These structural changes, representing a Jahn-Teller distortion of the d^2 configuration of Mo^{4+} from a regular octahedron to a distorted one, changes the ground state electronic structure of MoS_2 from being metallic in T phase to a small bandgap semiconductor in the T′ phase. Moreover, total energy calculations suggest that the distorted phase is relatively more stable compared to the undistorted state; in fact, the undistorted state is found to be unstable and is expected to spontaneously distort.

2. AFM study on the pristine and intercalated flakes:

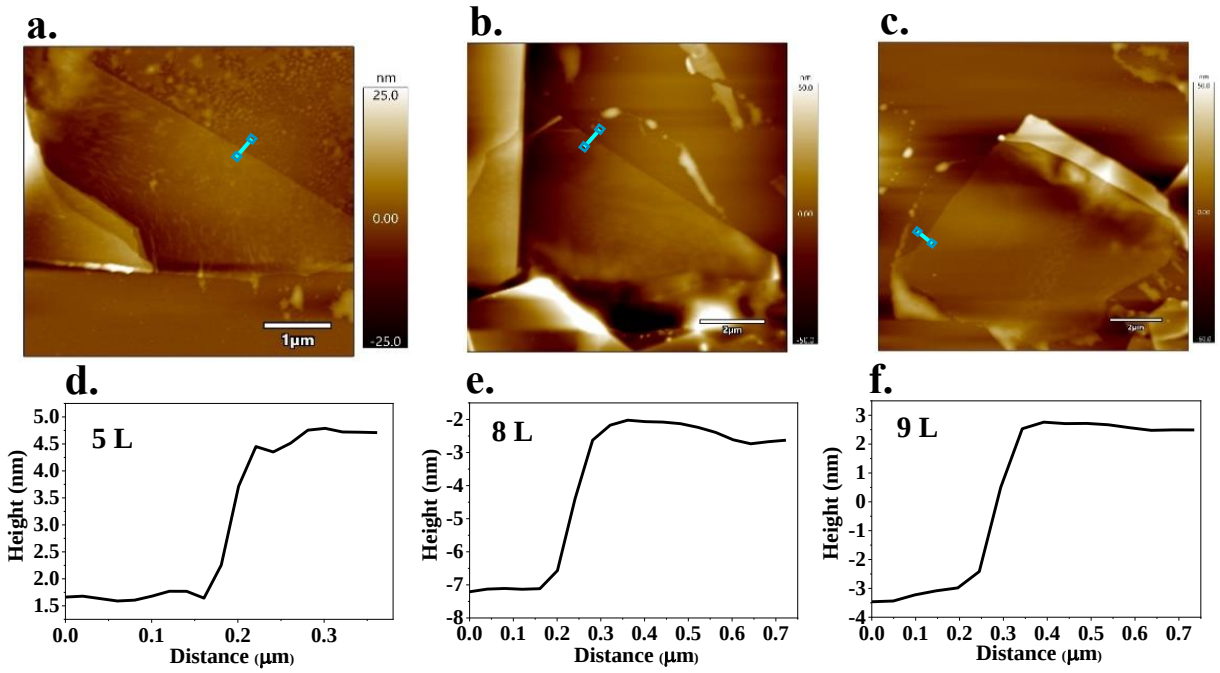

Fig. S2. (a), (b), (c) Representative AFM images of the pristine H samples and (d), (e), (f) corresponding height profiles of the flakes represented in (a), (b) and (c) respectively through the cyan lines.

Mechanically exfoliated H samples (Fig. S2) were found primarily in the range of 4-9 layers with characteristic layer separation of about 0.65 nm, as reported in the literature [1,2].

In order to illustrate the effect of Li^+ ion intercalation as well as washing these intercalated flakes, we show in Fig. S3 an individual flake of pristine H (also shown in Fig. S2c) sample before intercalation (Fig. S3a), after Li^+ intercalation (Fig. S3b) and after washing with water (Fig. S3c). It clearly shows that the interlayer separation is increased to nearly 1.7 nm on intercalation, which reduces somewhat to about 1.1 nm on substantial removal of Li^+ ions via washing, as has been reported in the literature [3]. These hugely enhanced interlayer separation decouples successive layers, leading to essentially non-interacting single layers of MoS_2 in these chemically treated samples.

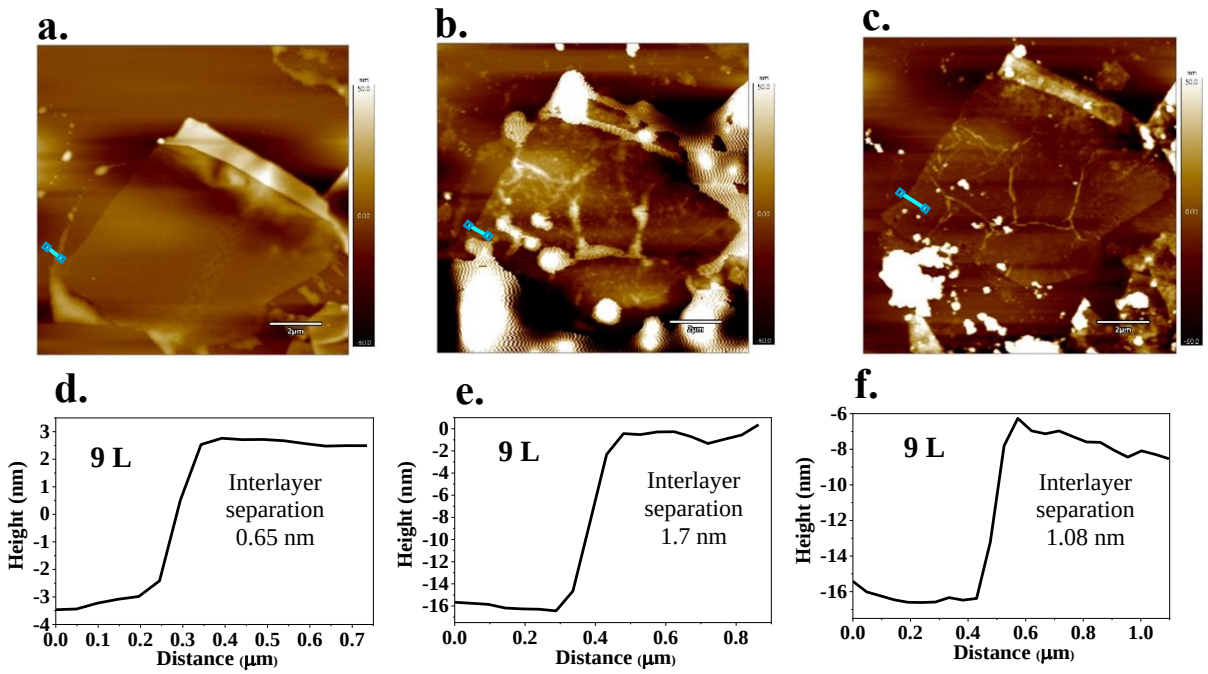

Fig. S3. Representative AFM images of an individual flake (a) before intercalation (H), (b) after Li^+ intercalation (0W) and (c) after washing (12W) with corresponding height profiles represented by the cyan lines shown in (d), (e) and (f) respectively.

3. Evidence for the presence of lithium ions (Li^+):

In Fig. S4, photoelectron spectra in the Li 1*s* region for the four chemically exfoliated samples, namely 0W, 1W, 6W and 12W, are presented along with the spectrum from the mechanically

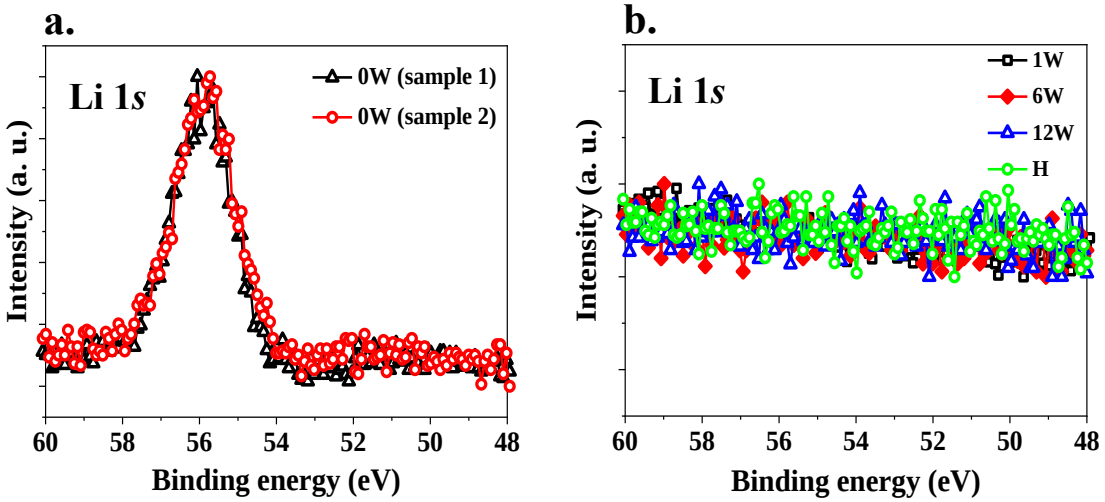

Fig. S4. Li 1*s* core level spectra for (a) 0W samples and (b) 1W, 6W and 12W and mechanically exfoliated pristine H samples.

exfoliated H sample. The 0W sample exhibits one peak, responsible for Li 1*s*, at binding energy of ~ 55.8 eV, shown in Fig. S4a normalized at the peak position. Two representative data, indicated by black and red lines, taken on different samples, are shown here in order to prove the reproducibility of the data. The spectrum in the binding energy window responsible for Li 1*s*, obtained from other chemically exfoliated samples apart from 0W and pristine H sample, are compared in Fig. S4b. It is quite clear that, only the noise level can be visible in Li 1*s* binding energy window for these samples, which further proves that the intercalated Li^+ ions react with water so vigorously that, even after a single wash the concentration level of Li^+ goes beyond the detection limit.

4. Raman spectra of the samples with different washing cycles:

We carried out preliminary studies for several control groups, namely 1W, 4W and 6W, in addition to 0W and 12W samples. The similarity of all washed samples is ascertained by the Raman spectra, shown in Fig. S5.

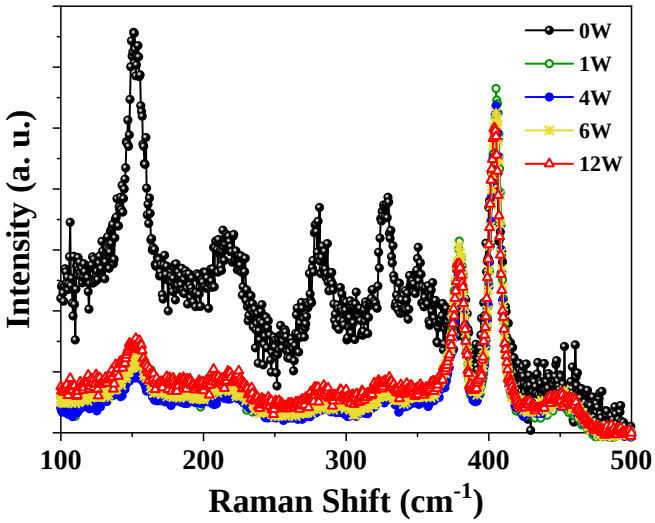

Fig. S5. Comparison of room temperature Raman spectra for the samples with different washing cycles normalized at 405 cm^{-1} (A_{1g} peak).

5. Photoelectron spectra of the samples with different washing cycles:

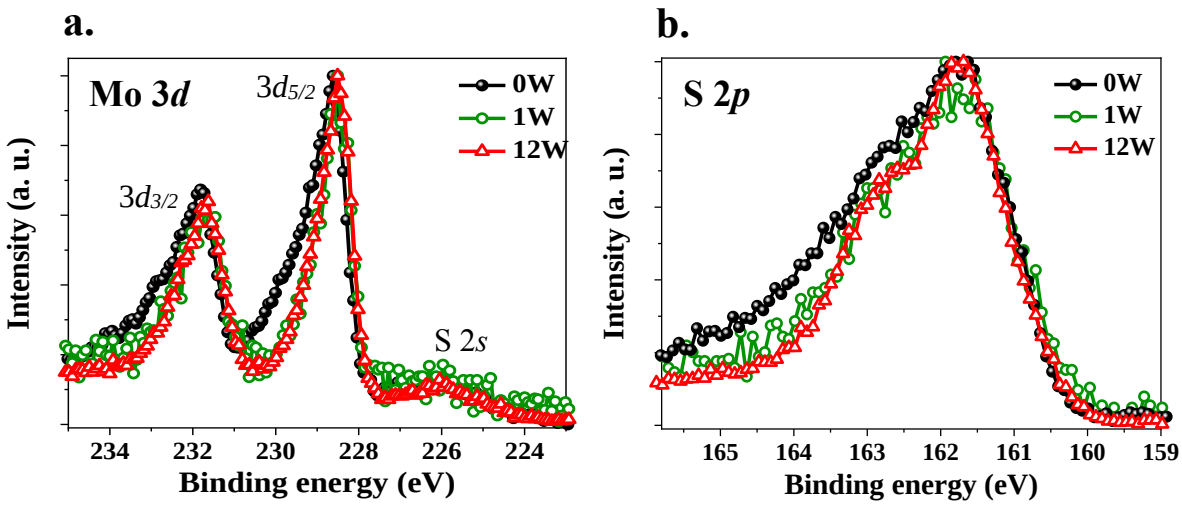

Fig. S6. Comparison of photoelectron spectra for 0W, 1W and 12W samples in the energy range of (a) Mo 3*d* and (b) S 2*p* core level.

The similarity of the two limiting washed samples, namely 1W and 12W, are distinct from the 0W sample in terms of their photoelectron spectroscopic results as shown in Fig. S6a and b.

6. Analysis of Raman spectrum from Group Theory point of view:

The presence of extra Raman peaks in intercalated samples can be explained with the help of Group Theory. The point groups, describing the symmetry of single MoS_2 layer of pristine H, T and T′ phases, are D_{3h}, D_{3d} and C_{2h} respectively. For each of the above mentioned point groups, irreducible representations corresponding to the normal modes of vibrations at zone centre (k = 0) along with the Raman and IR active modes are given below:

Table 1: Point group symmetry for different phases of MoS_2 along with the comparison between number of Raman active modes predicted from Group Theory and experimental observations.

Point group	**Irreducible representation**	**IR active**	**Raman active**	**No. of Raman modes**	**No. of prominent Raman peaks observed experimentally**
D_{3h}	$\Gamma_{vib}(\mathrm{H}) = A_1' + 2E' + 2A_2'' + E''$	E', A_2''	A_1', E', E''	3	Mostly 2. Presence of very weak E'' mode i.e. E_{1g} peak is reported in few studies[4,5].
D_{3d}	$\Gamma_{vib}(\mathrm{T}) = A_{1g} + E_g + 2E_u + 2A_{2u}$	E_u, A_{2u}	A_{1g}, E_g	2	2 peaks[5]
C_{2h}	$\Gamma_{vib}(\mathrm{T}') = 6A_g + 3B_g + 3A_u + 6B_u$	A_u, B_u	A_g, B_g	9	6 peaks*[6,7]

* Till now as per our knowledge there is no experimental report of stabilizing pure T′ phase. It is always coexisted with stable H phase. Therefore, it is inevitable to get signature of H phase in Raman spectroscopy, from the samples containing T′ phase. For such samples, three peaks responsible for H phase are accompanied by three more peaks, presumably coming from the presence of T′ phase.

7. Spectral fitting of 12W sample without plasmonic peak:

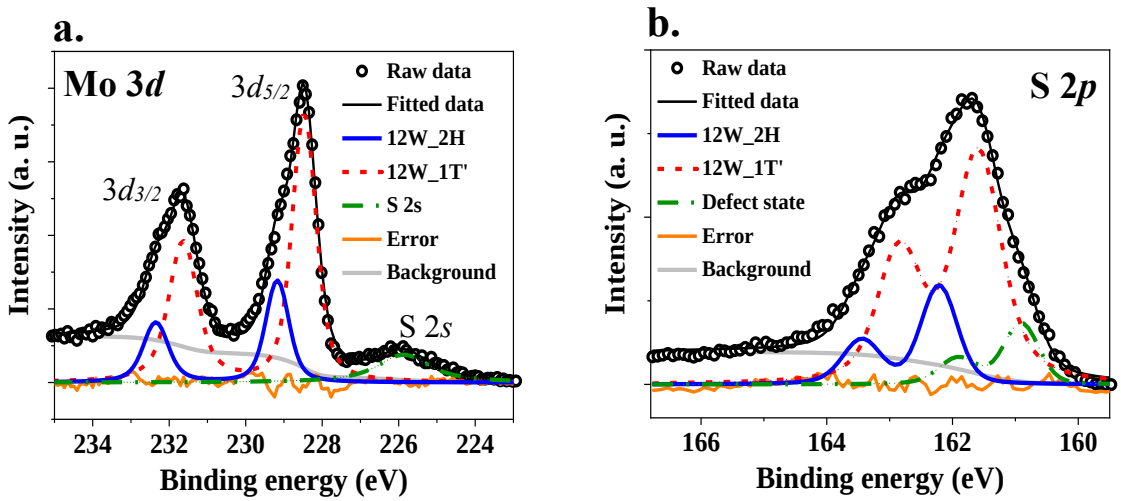

Fig. S7. Fitting of (a) Mo 3*d* and (b) S 2*p* core level spectra for 12W sample without considering the plasmon loss features.

Both Mo 3*d* and S 2*p* spectra obtained from 12W sample can be fitted with good agreement without considering the plasmon loss features, showing in Fig. S7. This clearly indicates towards almost non-existent nature of the plasmon satellites in 12W sample.

8. Fitting the core level spectra:

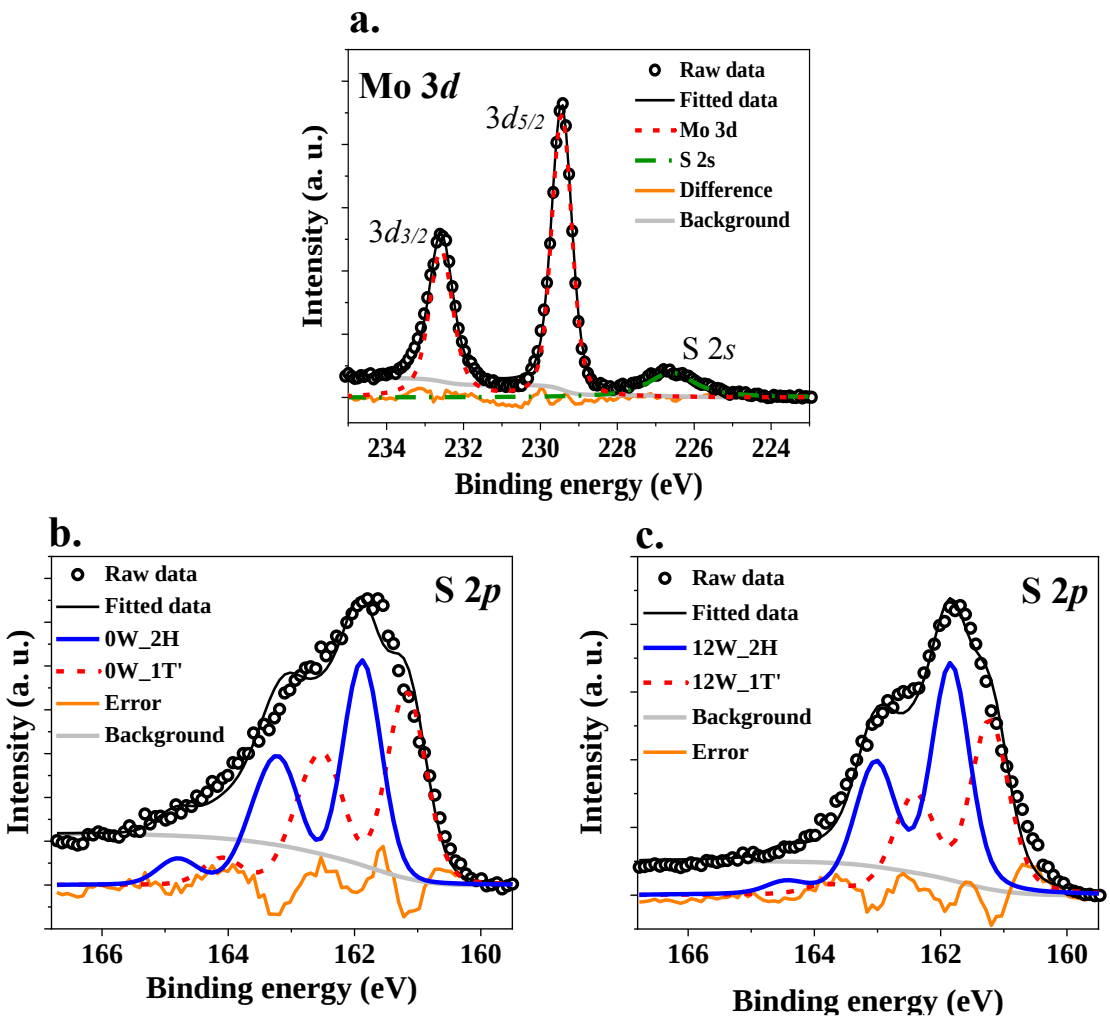

Fig. S8. (a) Fitted Mo 3*d* core level spectra obtained from mechanically exfoliated sample; S 2*p* core level spectra have been fitted with two components for (b) 0W and (c) 12W samples.

As there is only H phase present in mechanically exfoliated sample, the spectra can be decomposed in Mo $3d_{5/2}$, Mo $3d_{3/2}$ and S 2*s* component, showing in Fig. S8a. The shape of each peak is defined by a Lorentzian function convoluted by a Gaussian function, representing the lifetime and resolution broadening, respectively. Throughout our analysis we have used a single Gaussian broadening for all components, as the source of the resolution broadening lies in the instrumental artefact. We have imposed the constrain of fixed relative intensity between each spin orbit coupling pair i.e. the intensity ratio of $3d_{5/2}$ to $3d_{3/2}$ is 1.5 and similarly the intensity ratio between $2p_{3/2}$ and $2p_{1/2}$ is 2, along with the constant energy separation between each of these spin orbit pairs. We have used the least number of components required for a reasonable description of the Mo 3*d* and

S 2*p* spectra obtained from chemically exfoliated samples. As shown in Fig. S8a, only one component is sufficient to fit the spectra, while the Mo 3*d* spectra for both 0W and 12W samples can be fitted with the help of only two components, namely, H and T′ phase. It appears to be impossible to fit S 2*p* spectra assuming only two components as shown in Fig. S8b and c. For both 0W and 12W samples, the relative abundance of the H component is higher compared to that of the T′ component, which is contradicting the results obtained from Mo 3*d* fitting. The spin orbit coupling components in Mo 3*d* spectra are clearly distinguishable, indicating a much reliable fit in that case. On the contrary, $2p_{3/2}$ and $2p_{1/2}$ peaks are merged together for both the intercalated samples, making the fitting more difficult. In this scenario it is obvious to stick to the relative intensity value of the two components obtained from Mo 3*d* fitting, which in turn makes the S 2*p* spectral fitting with two components obsolete.

As described in the main text, in order to take care of the extra intensity, appearing in the higher binding energy side of each peaks in Mo 3*d* spectra of the 0W sample, we have assumed the presence of plasmon satellites. That can be easily done by defining a function, which is the summation of four Lorentzian functions. It is important to note that we have kept the intensity ratio fixed between two spin orbit coupling pairs of both the main and the plasmon peaks but the relative intensity between a main peak and its plasmon has been allowed to vary. Similarly, the peak positions have been varied in such a way that the distance from the main peak to its plasmon for both the spin orbit coupling components remain same.

References:

[1] M. Chhowalla, H.S. Shin, G. Eda, L.J. Li, K.P. Loh, H. Zhang, The chemistry of two-dimensional layered transition metal dichalcogenide nanosheets, Nat. Chem. 5 (2013) 263–275. https://doi.org/10.1038/nchem.1589.

[2] D. Wang, X. Zhang, S. Bao, Z. Zhang, H. Fei, Z. Wu, Phase engineering of a multiphasic 1T/2H MoS_2 catalyst for highly efficient hydrogen evolution, J. Mater. Chem. A 5 (2017) 2681–2688. https://doi.org/10.1039/C6TA09409K.

[3] X. Geng, W. Sun, W. Wu, B. Chen, A. Al-Hilo, M. Benamara, H. Zhu, F. Watanabe, J. Cui, T.P. Chen, Pure and stable metallic phase molybdenum disulfide nanosheets for hydrogen evolution reaction, Nat. Commun. 7 (2016) 1–7. https://doi.org/10.1038/ncomms10672.

[4] S. Jiménez Sandoval, D. Yang, R.F. Frindt, J.C. Irwin, Raman study and lattice dynamics of single molecular layers of MoS_2, Phys. Rev. B 44 (1991) 3955–3962. https://doi.org/10.1103/PhysRevB.44.3955.

[5] G. Zhu, J. Liu, Q. Zheng, R. Zhang, D. Li, D. Banerjee, D.G. Cahill, Tuning thermal conductivity in molybdenum disulfide by electrochemical intercalation, Nat. Commun. 7 (2016) 1–9. https://doi.org/10.1038/ncomms13211.

[6] F. Xiong, H. Wang, X. Liu, J. Sun, M. Brongersma, E. Pop, Y. Cui, Li Intercalation in MoS_2: In situ observation of its dynamics and tuning optical and electrical properties, Nano Lett. 15 (2015) 6777–6784. https://doi.org/10.1021/acs.nanolett.5b02619.

[7] B. Pal, A. Singh, G. Sharada, P. Mahale, A. Kumar, S. Thirupathaiah, H. Sezen, M. Amati, L. Gregoratti, U. V. Waghmare, D.D. Sarma, Chemically exfoliated MoS_2 layers: Spectroscopic evidence for the semiconducting nature of the dominant trigonal metastable phase, Phys. Rev. B 96 (2017) 1–7. https://doi.org/10.1103/PhysRevB.96.195426.